

APPLIED RESEARCH

An Automatic Method for Core Orientation Based on Planar Geologic Features in Drill-Core Scans and Microresistivity Images

SHUXIA ZHANG¹, CHENG PENG^{2,3}, AND CHANGCHUN ZOU^{2,3}¹Chinese Academy of Geological Sciences, Beijing 100037, China²School of Geophysics and Information Technology, China University of Geosciences, Beijing 100083, China³National Engineering Research Center of Offshore Oil and Gas Exploration, Beijing 100028, China

Corresponding author: Shuxia Zhang (sunny@cugb.edu.cn)


This work was supported in part by the Geological Survey Project of China under Grant DD20221677, in part by the Fundamental Research Funds for the Chinese Academy of Geological Sciences under Grant JKY202007, and in part by the Fundamental Research Funds for the Central Universities of China under Grant 2652019003.

ABSTRACT Drilling cores, the most direct and accurate first-hand data reflecting the subsurface geological information, are of unclear orientation for most boreholes. The image feature comparison method is one of the most widely used methods for core orientation. However, this method is mainly conducted by manual comparison, which is labor-intensive, time-consuming and inaccurate. In this paper, we propose an automatic core orientation method by comparing the planar geologic features (one of the most common features) in drill-core scans and microresistivity images. This method first automatically detects planar geologic features by combing the vertical gradient-based Otsu threshold segmentation, Hough transform and optimal sinusoid extraction and then determines correction difference of the core orientation by comparing the dip azimuths of the optimal sinusoids from the two types of images. This method is successfully applied to actual data. The automatic core orientation results are compared with the manual core orientation results. The results show that this method can eliminate human errors and has higher accuracy, especially for core scan images with non-distinct features. The proposed method has wide application potential in the fields of hydrocarbon exploration and development, scientific drilling research, and basic geological surveys.

INDEX TERMS Bedding surfaces, borehole images, core orientation, core scan images, Hough transform.

I. INTRODUCTION

The drilling core is the most direct and accurate first-hand data reflecting the subsurface geological information and plays an important role in hydrocarbon exploration and development, scientific drilling research, and basic geological surveys [1], [2], [3], [4]. The spatial orientation of the core is the key information and is the premise to determine the attitude of strata, fracture orientation, paleocurrent direction, in-situ stress direction, etc. [5], [6], [7], [8]. The direct orientation techniques of cores during drilling are expensive, time-consuming and sometimes inaccurate, so they have not been widely used [9], [10]. The drilling cores of most boreholes are of unclear orientation, which seriously affects the subsequent use and research of core data. Therefore, it is necessary to develop core orientation technology after drilling.

The associate editor coordinating the review of this manuscript and approving it for publication was Donato Impedovo .

The core orientation technology after drilling mainly includes two categories: paleomagnetic method and image feature comparison method. Although the paleomagnetic method has become more mature, there are still many defects, such as weak magnetism of cores, change of magnetization direction, sample contamination and other factors, both limit use and restrict confidence in orientation results [11], [12], [13]. The image feature comparison method orients the core mainly by comparing the geologic features of the core with those of the borehole wall [9], [10], [14], [15], [16], [17]. The planar geologic feature in core and borehole wall images is the best reference for the core orientation due to the following advantages: 1) These features generally correspond to bedding surfaces and fractures which are widely distributed in formations; 2) These features are stable at the drilling scale and appear on two types of images in similar patterns; 3) These features in core and borehole wall images generally appear as sinusoids, whose phase angles

are the vital parameters to determine their spatial azimuths. At present, the oriented borehole wall images can be obtained by microresistivity imaging logging, ultrasonic imaging logging and borehole optical televueing. Among these methods, microresistivity imaging logs have the advantages of high resolution and strong continuity, reflect the information of geologic features such as bedding surfaces and fractures, and thereby are widely used in core orientation [18], [19], [20]. Based on image feature comparison method, Zou et al. [21] developed an interactive program (CCSDLogCore) to determine the orientation of cores by human-computer interaction, but did not realize automatic core orientation. At present, the feature comparison between core and microresistivity images mainly relies on manual observation, which is not only labor-intensive and time-consuming, but there may also be human errors. Therefore, it is urgent to develop an automatic core orientation method by correlating planar geologic features in unoriented core images to those in microresistivity images.

The automatic detection and characterization of planar geologic features in core and borehole images are bases of automatic core orientation by comparing planar geologic features. Previous studies suggested that simple threshold segmentation methods are effective only in images with obvious differences between planar geologic features and background, such as the fracture segmentation in ultrasonic and borehole optical images (fractures tend to appear as dark sinusoidal curves) [22], [23], [24]. To accurately segment fractures from ultrasonic images with much background noise, previous researchers introduced methods such as mathematical morphology [25] and ant colony algorithm [26], [27], which greatly improved the effects of fracture segmentation. Unlike ultrasonic images mainly recording information about fractures and borehole breakouts, microresistivity images record abundant geologic features, and are more difficult to process [28], [29]. Assous et al. [30] utilized the phase consistency-based method for edge detection to realize the automatic extraction of planar geologic features from the microresistivity images. However, this method requires the pre-inpainting of gaps in the microresistivity images. For core and borehole images with abundant geologic features, some researchers employed machine learning methods to achieve relatively high detection precisions for fractures and unconformities [31], [32], [33], [34], [35].

After the image segmentation, it is necessary to extract the attitude information of the planar geologic features. Previous studies demonstrated that Hough transform is more robust in determining the dip angle and dip azimuth of fractures in borehole images than least squares fitting [36], [37], [38], [39], [40], [41]. However, the sinusoid detection using 3D Hough transform is computationally expensive. Zou and Shi [42] proposed a modified Hough transform using a 1D and a 2D transforms instead of a 3D transform, greatly improving the extraction efficiency of attitude information of planar geologic features from borehole images. Although the detection efficiency is high, the modified Hough transform has a low detection precision for incomplete fractures. To accurately identify non-distinct, partial, distorted

and steep fractures and layers, Waleed et al., [43] combined Gabor filter-based multi-resolution texture segmentation and pattern recognition techniques with iterative adaptation of Hough transforms. Wang et al. [44], [45] proposed an automatic recognition method of planar geologic features in borehole optical images based on iterative matching. However, previous studies mainly focused on the automatic extraction of fractures from borehole or core images. At present, the research on image processing technology for core orientation is still lacking.

Traditional interpretation of borehole and core images requires precise extraction of every single geologic feature in images, so it pays more attention to the differences of local geologic features. For this purpose, previous methods were developed for a certain type of image and focused on increasing the accuracy of feature detection and extracting the complex features (such as discontinuous and distorted fractures). Core orientation requires the comparison of significant macroscopic geologic features in the core and borehole images. Therefore, the automatic core orientation method focuses on detecting and extracting the macroscopic geologic features that appear on two types of images in similar patterns. In this paper, we propose an automatic core orientation method based on the macroscopic planar geologic features in the drill-core scans and microresistivity images.

II. DRILL-CORE SCANS AND MICRORESISTIVITY IMAGES

The core outer surface is scanned circumferentially by using a core scan equipment to obtain the rolled core scan image. The planar geologic features will be represented in the image by pixel color change. In addition to planar geologic features, there are human markers in the core image. After the core is taken out from the borehole, two longitudinal lines, red and black, will be drawn on its surface. These hand-drawn lines are azimuth reference lines. Generally, the red and black lines are respectively on the left and right, as the references for judging the top and bottom of the core. The purpose of core orientation technology after drilling is to determine the reliable azimuth of azimuth reference lines.

Microresistivity imaging logging tools obtain multiple apparent resistivity curves of the borehole wall in different directions by using the button electrodes on pads pressed against the borehole wall. Resistivity is one physical property of rocks. Microresistivity generally represents the resistivity of the flushed zone recorded by a microresistivity logging tool. Although various types of microresistivity imaging logging tools have been developed, they obtain microresistivity images using similar principles [46]. During logging, an applied voltage allows an alternating current to flow into the formation from each button electrode and to be received at the upper part of the tool. At the same time, the instrument records the current and applied voltage of the button electrode that reflect the change of borehole wall resistivity. The raw data acquired by microresistivity logging tools can be converted into microresistivity images after a series of pre-processing. The pre-processing mainly includes speed correction, eccentricity correction, normalization, etc. Here, we take the X-tended Range Micro Imager (XRMI) tool as an

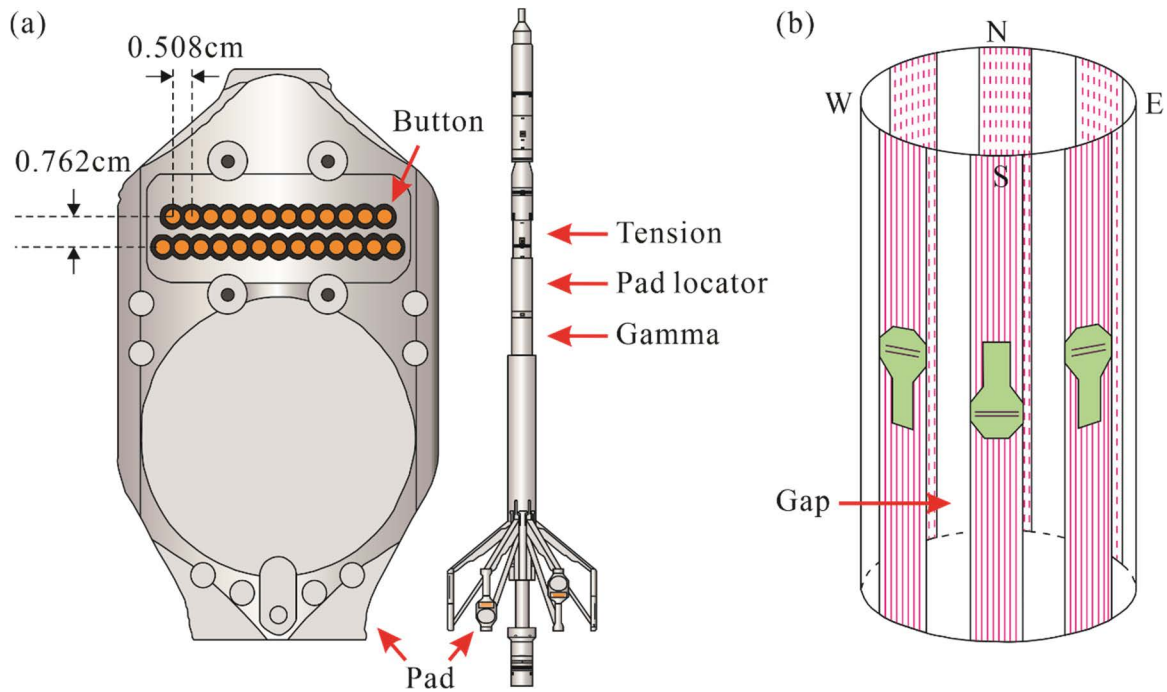


FIGURE 1. (a) X-tended Range Micro Imager tool; (b) Schematic diagram of data acquired by X-tended Range Micro Imager tool.

example to carry out our research. With 150 button electrodes on 6 pads, the XRMI tool simultaneously obtains 150 apparent resistivity curves (Fig. 1a). By converting the apparent resistivity into colors in normalization, a borehole wall image is formed. Conventionally, light and dark colors represent high and low values of apparent resistivity, respectively. Since the resistivity of formation is largely affected by its lithology and physical properties, beddings and fractures can be easily observed in microresistivity images. Since this tool includes a navigation package that provides accurate information on tool position and orientation within the borehole, it is possible to determine the dip angle and dip azimuth of planar geologic features in the image. However, due to the fixed pad area of the microresistivity imaging logging tool, there is a full circumferential coverage for the borehole wall of small-diameter wells. When the diameter of the borehole is large, there are uncovered areas between the pads appearing as longitudinal gaps in the image (Fig. 1b). Generally, for the XRMI tool, the larger the diameter of the borehole, the wider the gap is.

Due to the different image acquisition methods and targets, the microresistivity image is the mirror image of the core scan image. If the cylindrical microresistivity image is unwrapped in the true north direction, the resulting image has an orientation of “N-E-S-W-N” from left to right. If the cylindrical core scan image is unwrapped in the true north direction, the resulting image has an orientation of “N-W-S-E-N” from left to right. The planar geologic features appear as sinusoidal curves both in microresistivity images and core scan images (Fig. 2). Regardless of the difference in core and borehole sizes, the same bedding surface or fracture show a mirror image relationship in these two types of images.

III. METHOD

We propose a novel method to automatically orient the core by comparing the planar geologic features in the core scan image with those in the microresistivity image. This method mainly includes four steps: image segmentation, sinusoid detection, optimal sinusoid extraction and core orientation.

A. IMAGE SEGMENTATION

The objective of image segmentation is to separate the target region from the background. Most planar geologic features intersect the borehole obliquely. As a result, drill-core scans and microresistivity images vary significantly in the longitudinal direction. Although the edge detection algorithm can extract the layer boundaries, the result is affected by the gaps in microresistivity images and the vertical contaminants in core scan images. The threshold segmentation method can separate the light and dark areas in the image, but cannot extract the boundary of thick layers. To accurately segment planar geologic features from images, we employ a vertical gradient-based Otsu threshold segmentation method [47]. This method first calculates the vertical gradient of the image and then utilizes the Otsu threshold segmentation method to automatically segment the vertical gradient image. As a result, the binary image about the edge is obtained. Since the gaps in the microresistivity image are longitudinal, this method is free from the influence of the gaps. Therefore, there is no need for gap inpainting of the microresistivity image here.

There are abundant noise and non-distinct features in some core scan images. To improve the segmentation effect of these images, we first enhance contrast using histogram equalization and then conduct median filtering. Since the red and black lines, longitudinally penetrating the outer surface of

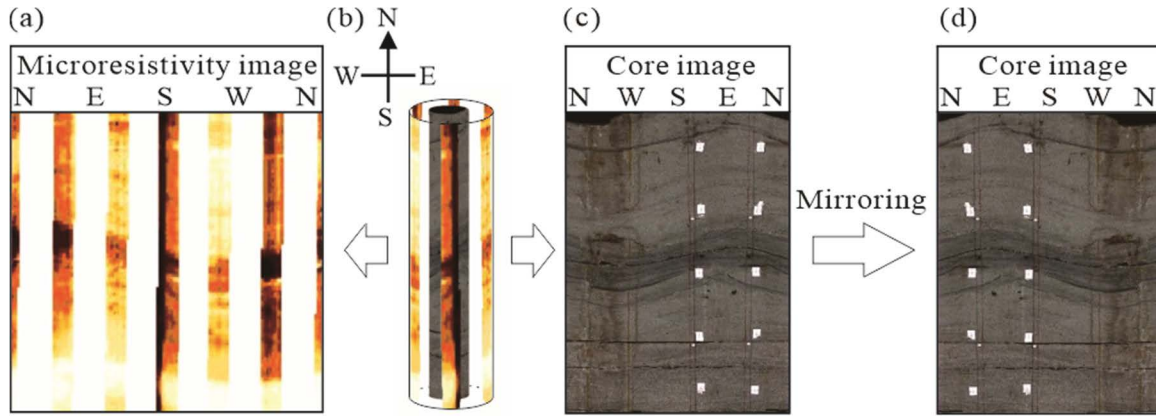


FIGURE 2. Drill-core scans and microresistivity images. (a) Unwrapped microresistivity image; (b) Wrapped microresistivity and core scan images; (c) Unwrapped core scan image; (d) Mirrored core scan image.

the core, were drawn before the core is scanned. These two important reference lines appear as longitudinal lines in the core scan image. Therefore, we utilize the horizontal gradient-based Otsu threshold segmentation method to obtain the binary image about the edge of reference lines. Hough transform is used to detect these reference lines [48].

B. SINUSOID DETECTION

We use the modified Hough transform to detect the sinusoidal curves in the microresistivity and core scan images. First, use odd symmetry to search for the baseline. Two points with a horizontal distance of a half period are used to obtain the 1D accumulator of the baseline position. Then, use a 2D accumulator to determine the amplitude and phase angle of the sinusoidal curve based on the baseline position.

In the microresistivity and core scan images, the planar geologic feature appears as a single-period sinusoidal curve. The sinusoidal curve can be expressed as:

$$y = A \sin(\omega x - \varphi) + y_0 \quad (1)$$

where, A is the sinusoid amplitude, φ is the phase angle, y_0 is the baseline position and ω is the angular frequency.

$$\omega = \frac{2\pi}{T} \quad (2)$$

The planar geologic features in microresistivity and core scan images are all one single-period sinusoids. The period T is known (that is, the number of horizontal points in the image). Therefore, there are three unknown parameters in the sinusoidal equation.

Assuming that the coordinates of two points P_1 and P_2 on the sinusoidal curve (S) are (x_1, y_1) and (x_2, y_2) , respectively. The horizontal interval between points P_1 and P_2 is half a period. Point C is the intersection of the line between points P_1 and P_2 and the baseline, and the coordinate of C is (x_c, y_c) (Fig. 3).

According to the odd symmetry of the sinusoid, the relationships between the coordinates of points P_1 and P_2 are as follows:

$$x_2 = x_1 + \frac{T}{2} \quad (3)$$

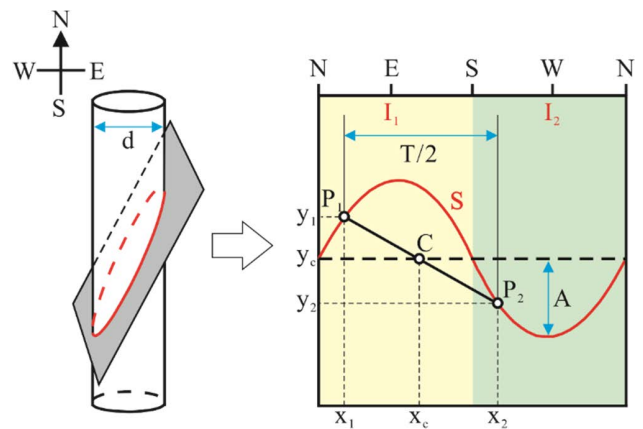


FIGURE 3. A single-period sinusoidal curve in mirrored drill-core scans and microresistivity images.

$$y_c = \frac{y_1 + y_2}{2} \quad (4)$$

According to (3) and (4), the baseline position can be obtained by using a 1D accumulator to accumulate the votes: 1) Divide the original image into two equal parts. The left part I_1 and the right part I_2 share the same width which is half the width of the original image (Fig. 3); 2) Visit a point $P(x_p, y_p)$ in I_1 , find all points P' which have horizontal coordinates of $x_p + T/2$ and vertical coordinate range of $y_p - A'$ to $y_p + A'$ (A' need to be greater than A) in I_2 ; 3) Calculate the vertical coordinate y_c of the midpoint of points P and P' , and cast a vote at y_c in the 1D accumulation space; 4) Repeat the steps 2 and 3, when all the points in I_1 have been visited, the calculation ends; 5) Find the local maximum values of the accumulator space by a given threshold, and each maximum corresponds to one baseline position.

After determining the baseline position of the sinusoid, extract the amplitude A and phase angle $\varphi \in [0, 2\pi]$ by using transform: 1) Create a 2D accumulator space according to the value ranges of amplitude A and phase angle φ ; 2) Visit a baseline position, make phase angle φ change from 0 to T (for a single-period sinusoid, $T = 2\pi$), calculate the corresponding amplitude A using (5), and cast votes in the 2D accumulator space according to the values of each pair

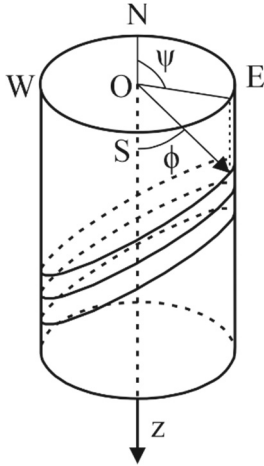


FIGURE 4. 3D coordinate system.

of amplitude and phase angle; 3) Repeat step 2, when all the baseline positions have been visited, the calculation ends; 4) Find the local maximum values of the accumulator space by a given threshold, and each maximum corresponds to one pair of amplitude and phase angle.

$$A = \frac{y - y_0}{\sin(\omega x - \varphi)} \tag{5}$$

C. OPTIMAL SINUSOID EXTRACTION

Using the above methods, the accumulators for y_0 , A and φ are constructed. However, there are generally multiple local maxima in the accumulator spaces, which is mainly caused by: 1) There may be multiple planar geologic features of different attitudes (including dip angle and dip azimuth) in the image; 2) The points belonging to different planar geologic features may be wrongly combined to a false sinusoid, causing false peaks in the accumulator space. To extract the information of the optimal attitude, we employ a least variance method. It is assumed that a series of planar geologic features parallel to each other are recorded in the image. In 3D space, they are a series of parallel slices (Fig. 4). Given a set of y_0 , A and φ , calculate the variance sum of each slice:

$$V = \frac{1}{\sum_{ij} m_{ij}} \sum_{m_{ij}=1} (f_{ij} - \overline{f(v_{ij})})^2 \tag{6}$$

where $\overline{f(v_{ij})}$ is the average value on each slice; f_{ij} is the value of each point on the slice; m_{ij} is the number of points. To judge whether the points in the image are from the same slice, we utilize the method of Mirkes [49]. This method can quickly search for the points from the same slice in a Cartesian coordinate system. In this system, the origin O is at the center of the upper surface of a cylinder and z -axis is the vertical axis. Each slice in 3D space is described by two parameters $\phi \in [0, \pi/2]$ and $\psi \in [0, 2\pi]$. ϕ is the angle that the normal vector \mathbf{n} of slices makes with the vertical axis and is equal to apparent dip angle. ψ is the angle between the projection of the normal onto the base of the cylinder and true north and the angle difference between it and apparent dip

azimuth is 180° (Fig. 4). For a vertical borehole, the apparent dip angle and apparent dip azimuth are respectively equal to the true dip angle and true dip azimuth of the slice. The borehole deviation correction is not involved in this study. Therefore, dip angle and dip azimuth are used in the following discussion. Therefore, ϕ and ψ of the slice have the following relationships with phase angle φ and amplitude A of the planar geologic feature in microresistivity image.

$$\psi = \begin{cases} \varphi + \frac{\pi}{2}, & \varphi \leq \frac{3\pi}{2} \\ \varphi - \frac{3\pi}{2}, & \varphi > \frac{3\pi}{2} \end{cases} \tag{7}$$

$$\phi = \tan^{-1} \left(\frac{2A}{d} \right) \tag{8}$$

where d is the diameter of the borehole or core. In the 3D coordinate system, the normal vector \mathbf{n} of the slice is expressed as:

$$x_n = \sin \phi \sin \psi, \quad y_n = \sin \phi \cos \psi, \quad z_n = \cos \phi \tag{9}$$

In 3D space, the coordinate of each point in the image can be calculated by the following equations:

$$x_{ij} = R \sin \frac{2\pi j}{N}, \quad y_{ij} = R \cos \frac{2\pi j}{N}, \quad z_{ij} = h(i - 1) \tag{10}$$

where h is the thickness of each slice, a constant equal to the spacing between two adjacent slices. For the same type of image data, h is the vertical sampling interval of the image. Therefore, for the vectors \mathbf{r}_{ij} from the origin O to the points in the same slice, the projection lengths of the vectors on the normal of the slice are equal. For each slice, the dot product of its normal vector \mathbf{n} and vector \mathbf{r}_{ij} is constant.

$$p_{ij} = \mathbf{n} \cdot \mathbf{r}_{ij} = R \sin \phi \cos \left(\psi - \frac{2\pi j}{N} \right) + h(i - 1) \cos \phi \tag{11}$$

Divide (11) by h , we get

$$v_{ij} = \frac{R}{h} \sin \phi \cos \left(\psi - \frac{2\pi j}{N} \right) + (i - 1) \cos \phi \tag{12}$$

The slice number can be obtained by rounding v_{ij} to the nearest integer. All points belonging to the same slice share the same number. In the actual calculation, we obtain multiple groups of candidate sinusoids by giving a low threshold in the accumulator space. Then we extract the optimal sinusoid from these candidate sinusoids by utilizing the above method. Typically, the optimal sinusoid has the minimum V and its phase angle represents the optimal dip azimuth of planar geologic features in this microresistivity (or core scan) image. The optimal dip azimuth can be used for the next step-core orientation. In addition, according to the information about optimal sinusoid, we can quickly search the points belonging to the same slice, calculate the average value of each slice and then reconstruct full-coverage image without gaps (Fig. 5).

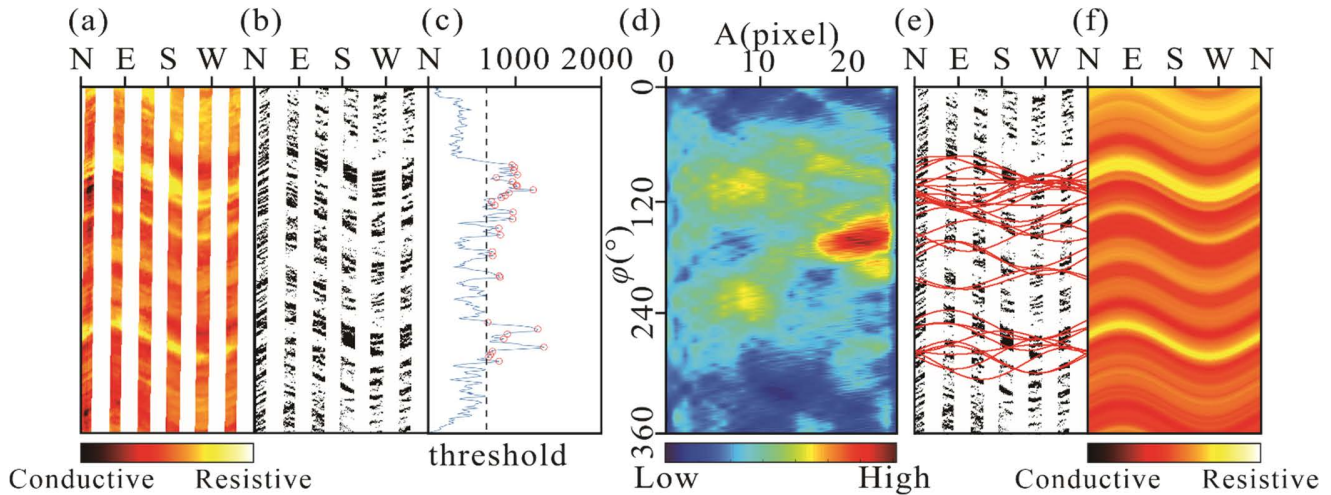


FIGURE 5. (a) Microresistivity image; (b) Segmentation results of microresistivity image; (c) 1D accumulator space for baseline position; (d) 2D accumulator space for amplitude and phase angle; (e) Automatic extraction results of sinusoid based on Hough transform; (f) Optimal sinusoid extraction.

D. CORE ORIENTATION

In the actual processing, considering the mirror image relationship between the core scan image and microresistivity image, the core scan image should be mirrored first, and then use the above method to obtain the optimal dip azimuths from the two types of images. The optimal dip azimuths obtained from the microresistivity image and the core scan image are named logging dip azimuth (φ_{log}) and core dip azimuth (φ_{core}), separately. Take the logging dip azimuth as the true dip azimuth and calculate the dip azimuth difference ($\varphi_{correct}$) between logging and core dip azimuths.

$$\varphi_{correct} = \varphi_{log} - \varphi_{core} \quad (13)$$

where $\varphi_{correct}$ is the correction difference of the core dip azimuth. When $\varphi_{correct}$ is positive, the core scan image should be turned to the right. When $\varphi_{correct}$ is negative, the core scan image should be turned to the left. The true dip azimuths of the red and black lines can be determined according to $\varphi_{correct}$.

$$\varphi_{line} = \begin{cases} \frac{2\pi j}{N} + \varphi_{correct} + 2\pi, & \frac{2\pi j}{N} + \varphi_{correct} < 0 \\ \frac{2\pi j}{N} + \varphi_{correct} - 2\pi, & \frac{2\pi j}{N} + \varphi_{correct} > 2\pi \\ \frac{2\pi j}{N} + \varphi_{correct}, & 2\pi > \frac{2\pi j}{N} + \varphi_{correct} > 0 \end{cases} \quad (14)$$

where N is the number of horizontal points in the core scan image; j is the j th point horizontally where the red or black line is located.

IV. RESULTS AND DISCUSSION

We present examples to objectively evaluate the performance of our method. The proposed method is first applied to the drilling core at depths of X263.7-X268.5 m of X well (Fig. 6). This interval is dominated by clastic rocks. With the increasing clay content, the rock color turns darker and the resistivity

decreases, causing darker colors in both the core scan and microresistivity images. The decrease of clay content corresponds to lighter colors in these two types of images. From top to bottom, there are multiple changes of lithology in this interval according to these two types of images. Macroscopically, several light-colored layers appear in the upper part of core B, the lower part of core C, the whole part of core D and the upper part of core F. All these light-colored layers have high values of resistivity, indicating the low clay content. Since the layers intersect the borehole obliquely, the layer boundaries appear as sinusoidal curves, which provides basic conditions for core orientation.

According to the microresistivity image, the optimal dip angle and dip azimuth of layers at depths of X263-X269 m barely change from top to bottom (Fig. 6a). Therefore, the proposed method is directly applied to the continuous microresistivity image of the whole interval for extraction of the optimal dip angle and dip azimuth of the layer boundaries. Theoretically, the dip angle and dip azimuth of layers in core scan image are consistent with those in microresistivity image. However, each drilling core being scanned has a length less than 1 m, resulting in discontinuity of the core scan image (Fig. 6h). Moreover, the orientation of the core scan image is unclear. Therefore, the proposed method is applied to each core scan image (core A-G), separately.

The results show that for the microresistivity and core scan images, whether there are obvious planar geologic features in them, the proposed method can accurately extract the optimal dip angle and dip azimuth from them (Fig. 6c, e). In addition, sometimes the drilling core is partially contaminated, resulting in some local planar geologic features being obscured partially or wholly in the core scan image. However, this phenomenon barely affects the extraction of the optimal sinusoid from the core scan image using the proposed method, which fully demonstrates that our method is robust. By comparing the microresistivity image and the core scan image, this method automatically calculates the correction difference

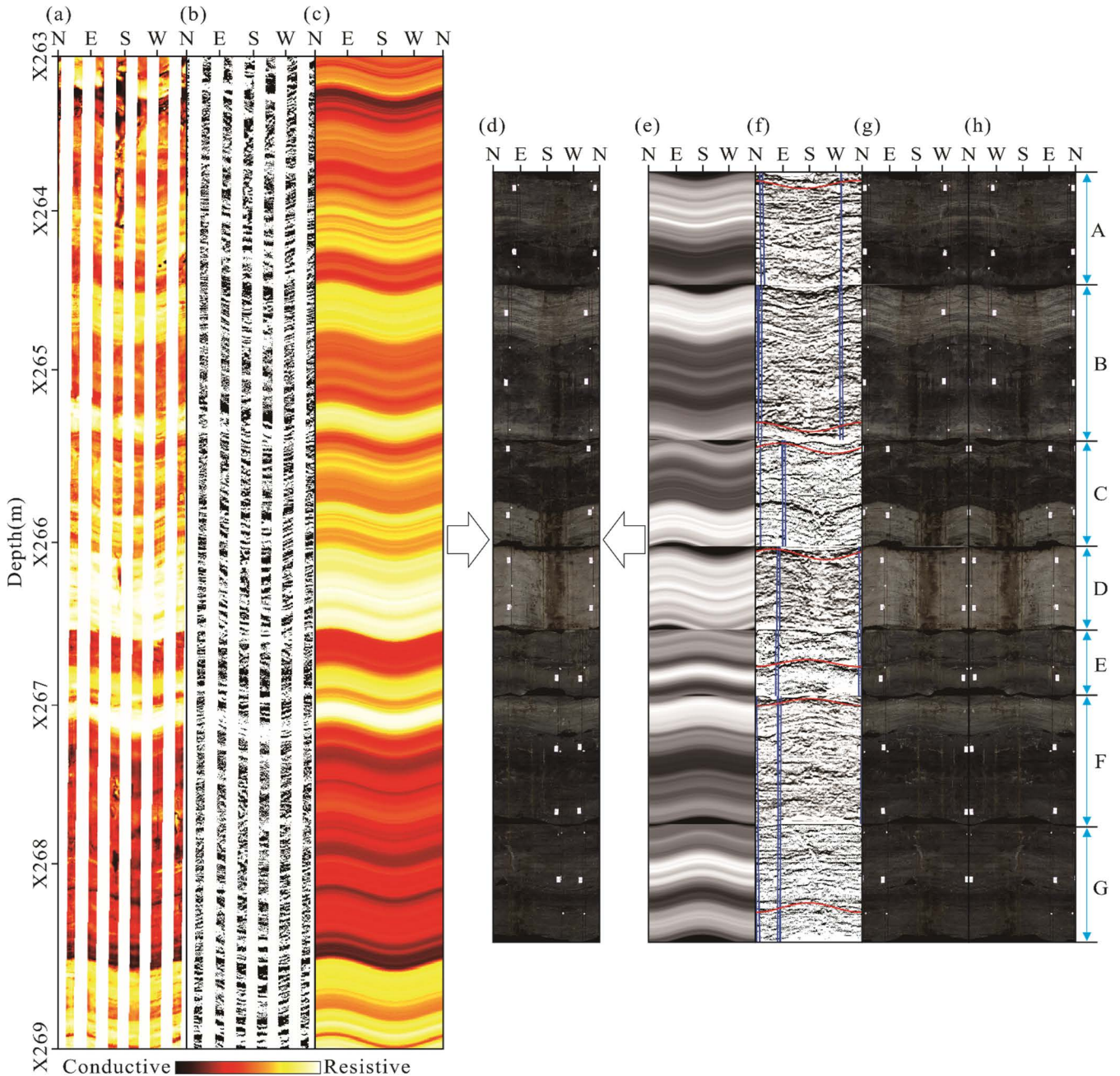


FIGURE 6. Automatic core orientation at depths of X263.0-X269.0 m of X well. (a) The microresistivity image; (b) The result of microresistivity image segmentation; (c) The reconstruction of the optimal sinusoid from the microresistivity image; (d) The core scan image after orientation; (e) The reconstruction of the optimal sinusoid from the core scan images; (f) The results of core scan image segmentation (the blue lines are the identified azimuth reference lines; the red lines are the extracted optimal sinusoid); (g) The core scan images after mirroring; (h) The original core scan images.

of the core orientation, thereby realizing the automatic orientation of the core (Fig. 6d).

The second example is shown in Fig. 7 where sedimentary beddings are well developed in the drilling core with a length of 2 m. There are dense dark bands alternate with light ones, which is the typical characteristic of sedimentary rocks. There is little difference in the dip angle among these beddings, so is in the dip azimuth (Fig. 7a). Therefore, we use the proposed method to process the continuous microresistivity image of the whole interval (Fig. 7b, c). The 2-meter-long core scan image, composed of the scan images of core H-J, is

discontinuous (Fig. 7h). Therefore, each core scan image (core H-J) is processed separately.

The results show that the optimal sinusoid extracted by our method basically reflects the distribution of the beddings. There are no obvious characteristics of sinusoidal curves in some intervals, such as the upper part of core H and the lower part of core I. However, this barely affects the core orientation. Because the small number of beddings with sinusoidal characteristics in the intervals have greater impact on the extraction of optimal sinusoid and dominate the extraction results. In some intervals, there are sinusoidal curves

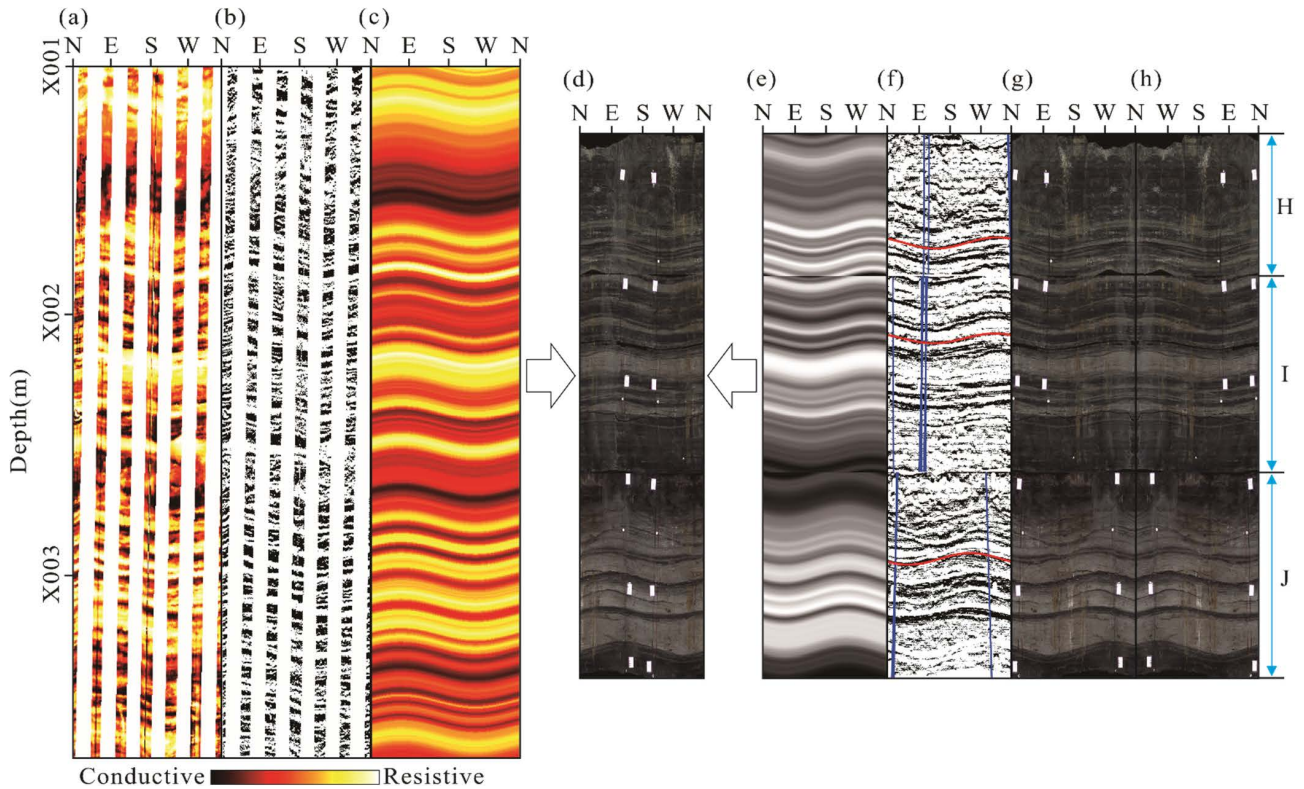


FIGURE 7. Automatic core orientation at depths of X001.0-X003.5 m of X well. (a) The microresistivity image; (b) The result of microresistivity image segmentation; (c) The reconstruction of the optimal sinusoid from the microresistivity image; (d) The core scan image after orientation; (e) The reconstruction of the optimal sinusoid from the core scan images; (f) The results of core scan image segmentation (the blue lines are the identified azimuth reference lines; the red lines are the extracted optimal sinusoid); (g) The core scan images after mirroring; (h) The original core scan images.

with different phase angle or amplitude. For example, in the upper part of core J, there is a sinusoidal curve the phase angle difference between which and other sinusoidal curves in this interval is 90° . Although this sinusoidal curve can be detected by the modified Hough transform, it is suppressed during extracting the optimal sinusoid, which indicates the robustness of our method.

The drilling cores in the above two examples have ever been manually orientated by the predecessors. These results obtained by the manual analysis method are compared with the automatic core orientation results obtained by using our method (Table 1). Since the dip azimuth range of the drilling core is $0\text{-}360^\circ$, the correction difference of 90° is equivalent to that of -270° . When comparing the correction difference from the manual analysis method and our method, turn all the correction differences into positive values, and calculate the relative error between the correction differences from the two methods.

Comparing the core orientation results of the manual analysis method and our method, it can be found that although the manual analysis method can determine the approximate orientation of the drilling core, there are errors in calculating the correction difference of dip azimuth. The errors are related to the planar geologic features in the core scan image. For the core scan images with obvious planar geologic features, the absolute errors between the correction differences from the two methods are generally less than 20° , and most relative error are less than 10%. The manual analysis

TABLE 1. Comparison of the orientation results obtained by using our method and the manual analysis method.

Core name	D1 ($^\circ$)	D2 ($^\circ$)	A ($^\circ$)	R (%)
A	65	34	-31	47.69
B	40	39	-1	2.50
C	326	318	-8	2.45
D	349	340	-9	2.58
E	234	340	106	45.30
F	223	180	-43	19.28
G	228	178	-50	21.93
H	113	102	-11	9.73
I	119	106	-13	10.92
J	191	206	15	7.85

Note: D₁ = correction difference of the core orientation using our method, D₂ = correction difference of the core orientation using the manual analysis method, A = the absolute error between the correction differences from the two methods, R = the relative error between the correction differences from the two methods

method depends on the judgement of the naked eye, and these errors are unavoidable. For the core scan images without obvious planar geologic features, these errors become very large. For some drilling cores, the relative errors between the correction differences from the two methods exceed 40%, and the absolute error exceeds 100° . Such large errors indicate that the core orientation result of the manual analysis method is almost wrong. This may be related to the following: 1) In the image, there are no planar geologic features obvious enough for the naked eye to recognize; 2) Different features are wrongly considered as the same one. The method

proposed in this paper can obtain the optimal sinusoid from the microresistivity and core scan images, which provides a powerful tool to avoid the above errors. This indicates that the accuracy of core orientation can be improved by using our method.

The workload of core orientation is enormous, especially for scientific drilling boreholes. For example, the main borehole of the Chinese Continental Scientific Drilling Project of the Cretaceous Songliao Basin (CCSD-SK) obtained abundant cores with a total length of 4135 m without using the direct orientation techniques of cores during drilling. Whether the core orientation is accurate will greatly affect the accuracy of scientific research results. The planar geologic feature which appears as a single-period sinusoidal curve, is the most common form of features in the microresistivity and core scan images. Therefore, the development of core orientation technology after drilling based on such sinusoidal features is of great significance. The core orientation technology will have broad applications, not only in the fields of hydrocarbon exploration and engineering application, but also in the field of scientific drilling. In addition, the optimal sinusoid extraction based on the modified Hough transform in our method can be applied to the gap inpainting and visualization of the microresistivity image.

V. CONCLUSION

Based on the comparison of the planar geologic features in drill-core scans and microresistivity images, we propose a new method for automatic core orientation. The feasibility of this method is verified by the application in actual data. The following conclusions are drawn:

1) This method can extract the optimal sinusoid and its dip angle and dip azimuth from the microresistivity and core scan images, with strong robustness and noise-suppressing capability. By comparing the dip azimuths of the optimal sinusoid from the two types of images, the core is orientated automatically. Considering the macroscopic planar geologic features in the image instead of the local ones, the core orientation results are of high accuracy.

2) From the comparison of the core orientation results obtained by using our method and the manual analysis method, there are errors in calculating the correction difference of core orientation for the latter method. The manual analysis method has bad ability to determine the orientation of the drilling core for the core scan images without obvious planar geologic features. Our method not only realizes the automatic core orientation, but also largely eliminate the error of manual orientation. Moreover, the accuracy of the core orientation using our method is improved for core scan images with non-distinct planar geologic features.

3) The proposed method is applicable to the core orientation of core scan images with planar geologic features. At present, microresistivity imaging logging and core scanning have been widely applied. Since bedding surfaces and fractures are widely distributed in formations, the planar geologic features are very common in these two types of images. Therefore, our method has wide application potential.

REFERENCES

- [1] T. Nian, Z. Jiang, G. Wang, C. Xiao, W. He, L. Fei, and Z. He, "Characterization of braided river-delta facies in the Tarim basin lower cretaceous: Application of borehole image logs with comparative outcrops and cores," *Mar. Petroleum Geol.*, vol. 97, pp. 1–23, Nov. 2018.
- [2] L. Pérez-Barnuevo, S. Lévesque, and C. Bazin, "Drill core texture as geometallurgical indicator for the Mont-Wright iron ore deposit (Quebec, Canada)," *Minerals Eng.*, vol. 122, pp. 130–141, Jun. 2018.
- [3] J. Westhoff, N. Stoll, S. Franke, I. Weikusat, P. Bons, J. Kerch, D. Jansen, S. Kipfstuhl, and D. Dahl-Jensen, "A stratigraphy-based method for reconstructing ice core orientation," *Ann. Glaciol.*, vol. 62, nos. 85–86, pp. 191–202, Nov. 2020.
- [4] C. Wang, Y. Gao, D. Ibarra, H. Wu, and P. Wang, "An unbroken record of climate during the age of dinosaurs," *Eos*, vol. 102, pp. 36–41, May 2021.
- [5] F. Fernández-Ibáñez, J. M. DeGraff, and F. Ibrayev, "Integrating borehole image logs with core: A method to enhance subsurface fracture characterization," *AAPG Bull.*, vol. 102, no. 6, pp. 1067–1090, Jun. 2018.
- [6] Y. Nagano, W. Lin, and K. Yamamoto, "In-situ stress analysis using the anelastic strain recovery (ASR) method at the first offshore gas production test site in the Eastern Nankai trough, Japan," *Mar. Petroleum Geol.*, vol. 66, pp. 418–424, Sep. 2015.
- [7] T. Nian, G. Wang, C. Xiao, L. Zhou, Y. Sun, and H. Song, "Determination of in-situ stress orientation and subsurface fracture analysis from image-core integration: An example from ultra-deep tight sandstone (BSJQK formation) in the Kelasu belt, Tarim basin," *J. Petroleum Sci. Eng.*, vol. 147, pp. 495–503, Nov. 2016.
- [8] J. M. Parés, N. J. C. Hassold, D. K. Rea, and B. A. van der Pluijm, "Paleo-occurrent directions from paleomagnetic reorientation of magnetic fabrics in deep-sea sediments at the Antarctic Peninsula Pacific margin (ODP sites 1095, 1101)," *Mar. Geol.*, vol. 242, no. 4, pp. 261–269, Aug. 2007.
- [9] T. S. Paulsen, R. D. Jarrard, and T. J. Wilson, "A simple method for orienting drill core by correlating features in whole-core scans and oriented borehole-wall imagery," *J. Struct. Geol.*, vol. 24, no. 8, pp. 1233–1238, Aug. 2002.
- [10] N. Shigematsu, M. Otsubo, K. Fujimoto, and N. Tanaka, "Orienting drill core using borehole-wall image correlation analysis," *J. Struct. Geol.*, vol. 67, pp. 293–299, Oct. 2014.
- [11] E. A. Hailwood and F. Ding, "Paleomagnetic reorientation of cores and the magnetic fabric of hydrocarbon reservoir sands," *Geol. Soc., London, Special Publications*, vol. 98, no. 1, pp. 245–258, Jan. 1995.
- [12] J. M. Parés, A. M. Schleicher, B. A. van der Pluijm, and S. Hickman, "Paleomagnetic reorientation of San Andreas fault observatory at depth (SAFOD) core," *Geophys. Res. Lett.*, vol. 35, no. 2, Jan. 2008, Art. no. L02306.
- [13] M. J. Pinto and M. McWilliams, "Drilling-induced isothermal remanent magnetization," *Geophysics*, vol. 55, no. 1, pp. 111–115, Jan. 1990.
- [14] E. Fontana, G. J. Iturrino, and P. Tartarotti, "Depth-shifting and orientation of core data using a core-log integration approach: A case study from ODP-IODP hole 1256D," *Tectonophysics*, vol. 494, nos. 1–2, pp. 85–100, Oct. 2010.
- [15] A. Genter, C. Castaing, C. Dezayes, H. Tenzer, H. Traineau, and T. Villemin, "Comparative analysis of direct (core) and indirect (borehole imaging tools) collection of fracture data in the hot dry rock Soultz reservoir (France)," *J. Geophys. Res., Solid Earth*, vol. 102, no. B7, pp. 15419–15431, Jul. 1997.
- [16] R. D. Jarrard, T. S. Paulsen, and T. J. Wilson, "Orientation of CRP-3 core, Victoria land basin, Antarctica," *Terra Antarctica*, vol. 8, no. 3, pp. 161–166, Feb. 2001.
- [17] S. F. Rogers, D. E. Bailey, and A. Kingdon, "Orientation of drill core by use of borehole geophysical imaging," *Appl. Earth Sci.*, vol. 109, no. 3, pp. 184–190, Dec. 2000.
- [18] A. Morris, J. S. Gee, N. Pressling, B. E. John, C. J. MacLeod, C. B. Grimes, and R. C. Searle, "Footwall rotation in an oceanic core complex quantified using reoriented integrated ocean drilling program core samples," *Earth Planet. Sci. Lett.*, vol. 287, nos. 1–2, pp. 217–228, Sep. 2009.
- [19] X. Nie, C. Zou, L. Pan, Z. Huang, and D. Liu, "Fracture analysis and determination of in-situ stress direction from resistivity and acoustic image logs and core data in the Wenchuan earthquake fault scientific drilling Borehole-2 (50–1370 m)," *Tectonophysics*, vol. 593, pp. 161–171, May 2013.
- [20] T. H. D. Payenberg, S. C. Lang, and R. Koch, "A simple method for orienting conventional core using microresistivity (FMS) images and a mechanical goniometer to measure directional structures on cores," *J. Sedimentary Res.*, vol. 70, no. 2, pp. 419–422, Mar. 2000.

- [21] C. C. Zou, L. Z. Pan, Y. X. Niu, H. P. Pan, and W. X. Wang, "Well log images for core location and reorientation, application to the main drillhole of the Chinese continental scientific drilling project," *J. China Univ. Geosci.*, vol. 18, pp. 1–3, Jun. 2007.
- [22] S.-K. Feng, T. Huang, and H.-J. Li, "Automatic identification of cracks from borehole image under complicated geological conditions," *J. Shanghai Jiaotong Univ., Sci.*, vol. 18, no. 6, pp. 699–705, Dec. 2013.
- [23] L. Li, C. Yu, Z. Han, and T. Sun, "Automatic identification of the rock-soil interface and solution fissures from optical borehole images based on color features," *IEEE J. Sel. Topics Appl. Earth Observ. Remote Sens.*, vol. 12, no. 10, pp. 3862–3873, Oct. 2019.
- [24] W. Zhang, T. Wu, Z. Li, S. Liu, A. Qiu, Y. Li, and Y. Shi, "Fracture recognition in ultrasonic logging images via unsupervised segmentation network," *Earth Sci. Informat.*, vol. 14, no. 2, pp. 955–964, Mar. 2021.
- [25] C. Peng, C. C. Zou, Z. Q. Lu, C. Q. Yu, A. Q. Liu, Y. Y. Tang, X. D. Hu, S. X. Zhang, H. J. Wen, Y. H. Li, and W. C. Wang, "Evidence of pore-and fracture-filling gas hydrates from geophysical logs in consolidated rocks of the Muli area, Qinghai–Tibetan plateau permafrost, China," *J. Geophys. Res., Solid Earth*, vol. 124, no. 7, pp. 6297–6314, Jul. 2019.
- [26] M. Liang, S. Peng, W. Du, and Y. Lu, "Tectonic stress estimation from ultrasonic borehole image logs in a coal bed methane well, Northeastern Qinshui basin, China," *J. Natural Gas Sci. Eng.*, vol. 52, pp. 44–58, Apr. 2018.
- [27] C. Peng and C. C. Zou, "Automatic extraction method for imaging logs crack based on improved ant colony algorithm," *Comput. Eng.*, vol. 8, no. 41, pp. 196–201, 2015.
- [28] M. Shafiabadi, A. Kamkar-Rouhani, S. R. Ghavami Riabi, A. R. Kahoo, and B. Tokhmechi, "Identification of reservoir fractures on FMI image logs using Canny and Sobel edge detection algorithms," *Oil & Gas Sci. Technol.-Revue D'IFP Energies nouvelles*, vol. 76, p. 10, Feb. 2021.
- [29] M. Shafiabadi, A. Kamkar-Rouhani, and S. M. Sajadi, "Identification of the fractures of carbonate reservoirs and determination of their dips from FMI image logs using Hough transform algorithm," *Oil & Gas Sci. Technol.-Revue D'IFP Energies nouvelles*, vol. 76, p. 37, Jun. 2021.
- [30] S. Assous, P. Elkington, S. Clark, and J. Whetton, "Automated detection of planar geologic features in borehole images," *Geophysics*, vol. 79, no. 1, pp. D11–D19, Jan. 2014.
- [31] F. Alzubaidi, P. Makuluni, S. R. Clark, J. E. Lie, P. Mostaghimi, and R. T. Armstrong, "Automatic fracture detection and characterization from unwrapped drill-core images using mask R-CNN," *J. Petroleum Sci. Eng.*, vol. 208, Jan. 2022, Art. no. 109471.
- [32] L. O. Dias, C. R. Bom, E. L. Faria, M. B. Valentin, M. D. Correia, M. P. de Albuquerque, M. P. de Albuquerque, and J. M. Coelho, "Automatic detection of fractures and breakouts patterns in acoustic borehole image logs using fast-region convolutional neural networks," *J. Petroleum Sci. Eng.*, vol. 191, Aug. 2020, Art. no. 107099.
- [33] F. Taibi, G. Akbarizadeh, and E. Farshidi, "Robust reservoir rock fracture recognition based on a new sparse feature learning and data training method," *Multidimensional Syst. Signal Process.*, vol. 30, no. 4, pp. 2113–2146, Apr. 2019.
- [34] S. Yang, H. Li, L. Ma, and W. Bai, "An automatic method for discontinuity recognition in coal-measure strata borehole images," *IEEE Access*, vol. 9, pp. 105072–105081, 2021.
- [35] W. Zhang, T. Wu, Z. P. Li, Y. J. Li, A. Qiu, and Y. B. Shi, "Automatic detection of fractures based on optimal path search in well logging images," *J. Sens.*, vol. 2021, p. 5577084, Sep. 2021.
- [36] K. Glossop, P. J. G. Lisboa, P. C. Russell, A. Siddans, and G. R. Jones, "An implementation of the Hough transformation for the identification and labelling of fixed period sinusoidal curves," *Comput. Vis. Image Understand.*, vol. 74, no. 1, pp. 96–100, Apr. 1999.
- [37] J. Hall, M. Ponzi, M. Gonfalini, and G. Maletti, "Automatic extraction and characterization of geological features and textures from borehole images and core photographs," in *Proc. 37th Annu. Logging Symp.*, New Orleans, LA, USA, 1996, pp. 1–13.
- [38] B. B. Thapa, P. Hughett, and K. Karasaki, "Semi-automatic analysis of rock fracture orientations from borehole wall images," *Geophysics*, vol. 62, no. 1, pp. 129–137, Jan. 1997.
- [39] D. Torres, R. Strickland, and M. Gianzero, "A new approach to determining dip and strike using borehole images," in *Proc. 31st Ann. Logging Symp.*, Lafayette, LA, USA, Jun. 1990, pp. 1–10.
- [40] M. van Ginkel, M. A. Kraaijveld, L. J. Van Vliet, E. P. Reding, P. W. Verbeek, and H. J. Lammers, "Robust curve detection using a Radon transform in orientation space applied to fracture detection in borehole images," in *Proc. 7th Annu. Conf. Adv. School Comput. Imag.*, R. L. Lagendijk, Eds. Delft, The Netherlands, May 2000, pp. 299–306.
- [41] S. A. Wong, R. A. Startzman, and T.-B. Kuo, "Enhancing borehole image data on a high-resolution PC," in *Proc. Petroleum Comput. Conf.*, 1989, pp. 37–48.
- [42] Z. Changchun and S. Ge, "A Hough transform-based method for fast detection of fixed period sinusoidal curves in images," in *Proc. 6th Int. Conf. Signal Process.*, 2002, pp. 909–912.
- [43] W. Al-Sit, W. Al-Nuaimy, M. Marelli, and A. Al-Ataby, "Visual texture for automated characterisation of geological features in borehole televiwer imagery," *J. Appl. Geophys.*, vol. 119, pp. 139–146, Aug. 2015.
- [44] C. Wang, X. Zou, Z. Han, Y. Wang, and J. Wang, "An automatic recognition and parameter extraction method for structural planes in borehole image," *J. Appl. Geophys.*, vol. 135, pp. 135–143, Dec. 2016.
- [45] C. Wang, X. Zou, Z. Han, J. Wang, and Y. Wang, "The automatic interpretation of structural plane parameters in borehole camera images from drilling engineering," *J. Petroleum Sci. Eng.*, vol. 154, pp. 417–424, Jun. 2017.
- [46] J. Lai, G. Wang, S. Wang, J. Cao, M. Li, X. Pang, C. Han, X. Fan, L. Yang, Z. He, and Z. Qin, "A review on the applications of image logs in structural analysis and sedimentary characterization," *Mar. Petroleum Geol.*, vol. 95, pp. 139–166, Aug. 2018.
- [47] N. Otsu, "A threshold selection method from gray-histogram," *IEEE Trans. Syst., Man, Cybern.*, vol. SMC-9, no. 1, pp. 62–66, Jan. 1979.
- [48] P. V. C. Hough, "Method and means for recognizing complex patterns," U.S. Patent 1 218, 1962.
- [49] E. M. Mirkes, A. N. Gorban, J. Levesley, P. A. S. Elkington, and J. A. Whetton, "Pseudo-outcrop visualization of borehole images and core scans," *Math. Geosci.*, vol. 49, no. 8, pp. 947–964, Sep. 2017.



SHUXIA ZHANG received the B.S. degree in geophysics and the M.S. degree in geological engineering from the China University of Geosciences, Wuhan, Hubei, China, in 2013 and 2015, respectively, and the Ph.D. degree in earth detection and information technology from the China University of Geosciences, Beijing, China, in 2019. She is currently a Postdoctoral Researcher with the Chinese Academy of Geological Sciences. Her research interests include petrophysics, geophysical logging, unconventional resources, and image processing.



CHENG PENG received the B.S. and Ph.D. degrees in geophysics from the China University of Geosciences, Beijing, China, in 2014 and 2019, respectively. He is currently a Lecturer with the School of Geophysics and Information Technology, China University of Geosciences. His research interests include geophysical logging, petrophysics, unconventional resources, and image processing.



CHANGCHUN ZOU received the B.S. degree in geophysical logging from Jiangnan Petroleum University, Jingzhou, Hubei, China, in 1992, the M.S. degree in geophysical logging from the Research Institute of Petroleum Exploration and Development, CNPC, Beijing, China, in 1997, and the Ph.D. degree in applied geophysics from the China University of Geosciences, Beijing, in 2000.

He is currently a Professor with the School of Geophysics and Information Technology, China University of Geosciences, where he is a Leader with the Geophysical Logging Laboratory. He also leads the Wellbore Detection Technology Research Sub-Center of Offshore Oil and Gas Exploration. His research interests include petrophysics, borehole geophysics, gas hydrate and hot dry rock exploration, and scientific drilling.

• • •